Characterization of the accuracy of EUV phase-shifting point diffraction interferometry

Patrick Naulleau[a], Kenneth Goldberg[a], Sang Lee[a, b], Chang Chang[a, b], Cynthia Bresloff[a], Phillip Batson[a], David Attwood[a, b], and Jeffrey Bokor[a, b]

[a] Center for X-Ray Optics, Lawrence Berkeley National Laboratory, Berkeley, CA 94720
[b] EECS Department, University of California, Berkeley, CA 94720

ABSTRACT

The phase-shifting point diffraction interferometer (PS/PDI) has recently been developed and implemented at Lawrence Berkeley National Laboratory to meet the significant measurement challenge of characterizing extreme ultraviolet (EUV) projection lithography systems. Here progress on the characterization of the PS/PDI accuracy is presented. Two major classes of errors affect the accuracy of the interferometer: the first being systematic effects arising from the measurement geometry, and the second being random and systematic errors caused by an imperfect reference wave. In order to characterize these contributions and calibrate the interferometer, a null test is required. This null test also serves as a measure of the absolute accuracy of the interferometer. Experimental results demonstrating a systematic-error-limited accuracy of 0.004 waves (λ/250 or 0.05 nm at λ = 13.4 nm) is reported.

Keywords: interferometry, point diffraction interferometry, extreme ultraviolet lithography, phase-shifting interferometry, accuracy.

1. INTRODUCTION

Interferometric testing is a necessary tool for the development of diffraction limited extreme ultraviolet (EUV) lithographic optical systems. Because these systems utilize resonant reflective multilayer-coated optics, interferometry using the lithographic operational wavelength is essential. EUV lithographic systems require fabrication tolerances on the order of 0.02 waves rms (0.3 nm rms at a wavelength of 13.4 nm).[1] Such tolerances place extremely high demands on the at-wavelength interferometric testing, which must provide measurement accuracy on the order of 0.01 waves (λ/100 or 0.1 nm). The phase-shifting point diffraction interferometer (PS/PDI), recently developed and implemented at Lawrence Berkeley National Laboratory, has been designed to meet this significant measurement challenge. At-wavelength interferometric measurement of reflective EUV optical systems has also been reported using lateral-shearing interferometry,[2] Foucault, and Ronchi testing.[3]

The two primary sources of measurement errors that limit the absolute accuracy of the PS/PDI are imperfections in the reference wave generated by the image plane pinhole and systematic effects that arise from the geometry of the system. The systematic geometric effects can be removed, providing they can be accurately measured. The reference-pinhole-induced errors are much more difficult to remove through calibration because they depend on the shape and position of the reference pinhole and also on the aberrations present in the test optic; however, the random contribution of these errors can be suppressed through averaging.

In order to characterize the errors described above, and hence calibrate the PS/PDI, a null test is required. Analogous to Young's classic two-slit experiment, a null test can be performed on the PS/PDI by placing a two-pinhole "null-mask" in the image plane. In the null test case, two high quality spherical waves are generated by diffraction from the image plane mask creating a fringe pattern (interferogram) in the far field of the mask.

Aberrations measured from this null-mask interferogram are indicative of the systematic and random errors in the interferometer.

2. PS/PDI DESCRIPTION

The PS/PDI is briefly described here; a more complete description can be found in the literature.[4-7] The PS/PDI is a variation of the conventional point diffraction interferometer in which a transmission grating has been added to greatly improve the optical throughput of the system and add phase-shifting capability. In the PS/PDI (Fig. 1), the optical system under test is illuminated by a spherical wave generated by a pinhole placed in the object plane of the system under test. To guarantee the quality of the spherical wave illumination, the pinhole is chosen to be several times smaller than the resolution limit of the optical system. The grating splits the illuminating beam to create the required test and reference beams. A mask (referred to as the "PS/PDI mask") is placed in the image plane of the optical system under test to block the unwanted diffracted orders generated by the grating and to spatially filter the reference beam using a pinhole (the "reference pinhole"). The test beam, containing the aberrations imparted by the optical system, is largely undisturbed by the image plane mask by virtue of it passing through a large (relative to the point spread function of the optical system) window in the PS/PDI mask. The test and reference beams propagate to the mixing plane where they overlap to create an interference pattern recorded on a CCD detector. The recorded interferogram yields information on the deviation of the test beam from the reference beam which in the ideal case is a spherical wave.
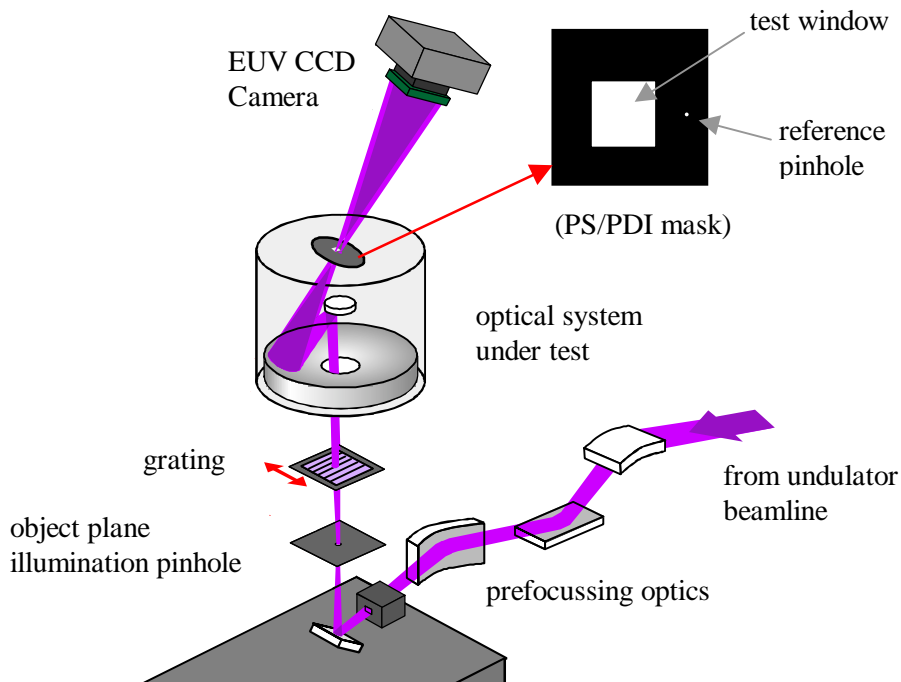

Fig. 1. PS/PDI configuration for the measurement of a 10×-demagnifying Schwarzschild objective.

3. NULL-TEST DESCRIPTION

Based on the description above, if the optic under test were perfect (generating a perfect spherical wave) the interferogram would consist solely of a uniform spatial frequency fringe pattern. Ignoring the tilt term, the reconstructed difference wavefront would be uniform. When examined in greater detail however, even with a perfect optic there would be deviations from a uniform spatial frequency fringe pattern simply due to the geometry

of the interferometer and the absence of re-imaging optics. Furthermore, when the optic is not perfect, the quality of reference beam depends upon how well the reference pinhole spatially filters the aberrations from the optic. These two effects limit how accurately an uncalibrated PS/PDI can measure the wavefront of a system under test. In practice the absolute measurement accuracy of the interferometer can be improved through a calibration process.

In order to calibrate the interferometer and determine its accuracy, a null test is required. A natural way to implement the PS/PDI null test is to replace the PS/PDI mask with a null-mask. In the null-mask the large (typically 4.5 μm) test window is replaced by a second pinhole identical to the reference pinhole. These pinholes are usually in the 80 to 150-nm diameter range. Figure 2 shows scanning electron microscope images of a standard PS/PDI mask [Fig. 2(a)] and a null-mask [Fig 2(b)]. These masks were fabricated using electron beam lithography and reactive ion etching. The masks are made up of a 200-nm thick Ni absorbing layer evaporated on 100 nm Si_3N_4 membranes. The mask features are etched completely through the membrane prior to the Ni evaporation. Thus the pinholes and windows are completely open in the finished masks, which maximizes their transmission. With the null-mask in place, both the test and reference beams are spatially filtered creating two nearly spherical waves.
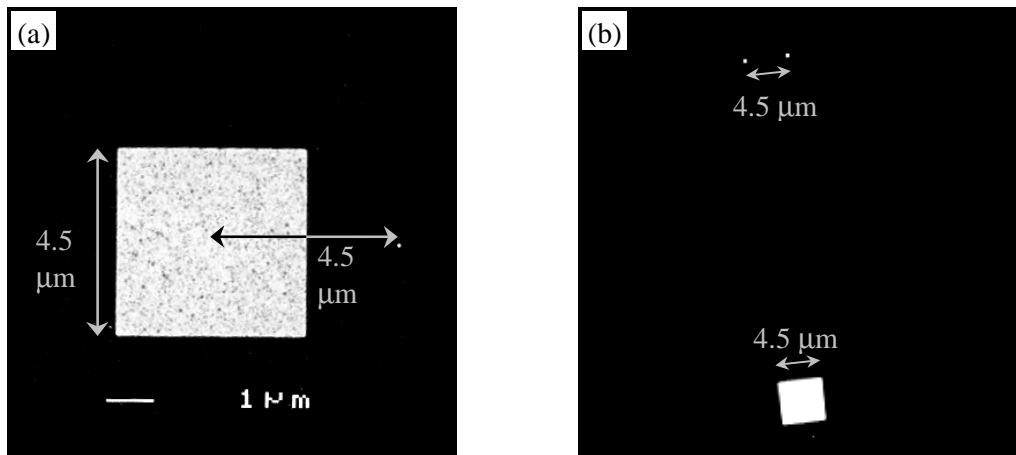

Fig. 2. Scanning electron microscope images of (a) a standard PS/PDI mask and (b) a null-mask. The square window in (a) is the test beam window and the reference pinhole to the right has a diameter <100 nm. In (b) we see the pinhole pair (~120-nm diameter each) along with an alignment window ~40 μm below the pinholes.

We note that this test is limited to characterizing errors originating at or after the image plane. Although there may be error-inducing geometric effects before the image plane (for example from the illumination of a planar uniform-pitch grating with a spherical wave), these errors are small compared the geometric errors considered here and will be ignored.[8] Another potential source of pre-image-plane error is the object pinhole which generates a spherical illumination wave by spatial filtering the undulator radiation. The object pinhole quality can be quantified using a similar two-pinhole test. In general, the object pinhole requirements, in terms of pinhole size and shape, are much less severe and easier to achieve than are those for the image plane pinhole. This is because the optical systems being tested are demagnifying systems. The accuracy measurements presented here are based on the use of suitably high quality object pinholes verified by other tests not discussed here. Commercially available laser-drilled pinholes of 0.5-μm diameter are used for the object pinhole in these experiments.

4. GEOMETRICAL COMA SYSTEMATIC EFFECT

For the EUV PS/PDI with an image side numerical aperture (*NA*) < 0.1, the largest geometric effect is coma which arises due to the large amount of shear between two nominally spherical wavefronts. The magnitude of this

error can readily be found analytically by considering the path length difference from two point sources [separated laterally by a distance s equal to the image point (pinhole) separation in the image plane] to a point in the mixing (detector) plane (Fig. 3). Without loss of generality we assume the point separation s to lie along the x-axis. Expressing r_1 and r_2, from Fig. 3, as second order binomial expansions and considering the path length difference ($\Delta R = r_1 - r_2$), as a function of mixing plane position in polar coordinates (ρ, θ), we obtain

$$\Delta R = \left(\frac{s}{2z^3} \rho^3 - C\rho \right) \cos\theta , \qquad (1)$$

where C is the constant representing the linear phase (spatial carrier) term and z is the distance from the image plane to the mixing plane. We note that a first order expansion of r_1 and r_2 (the Fresnel approximation) is not accurate enough to determine the geometric coma effect being sought here.

From Eq. (1) we find the geometric coma to lie in the direction of the pinhole separation and to have a Zernike coefficient magnitude of

$$e_c = \frac{s}{6} \left(\frac{r_m}{z} \right)^3 , \qquad (2)$$

where r_m is the maximum radial (lateral) extent of the measurement at the mixing plane (all aberration magnitudes presented here are defined as zero-to-peak values unless otherwise stated). Equation (2) can be rewritten in terms of NA and simplified using the small angle approximation yielding,

$$e_c = \frac{s}{6} \tan^3 \left[\sin^{-1}(NA) \right] \approx \frac{1}{6} s\, NA^3 . \qquad (3)$$

Figure 4 shows a plot of the theoretical geometric coma as a function of NA. The pinhole separation, s, is set to the typical experimental value of 4.5 μm. For current EUV lithographic Schwarzschild testing we are interested in numerical apertures between 0.06 and 0.1. For these values, the geometric coma effect limits the uncalibrated interferometer to a measurement accuracy ranging from 0.16 nm to 0.75 nm, respectively. Calibrating the interferometer to remove this geometric coma term is clearly required to achieve the desired

Fig. 3. Measurement geometry leading to systematic coma.
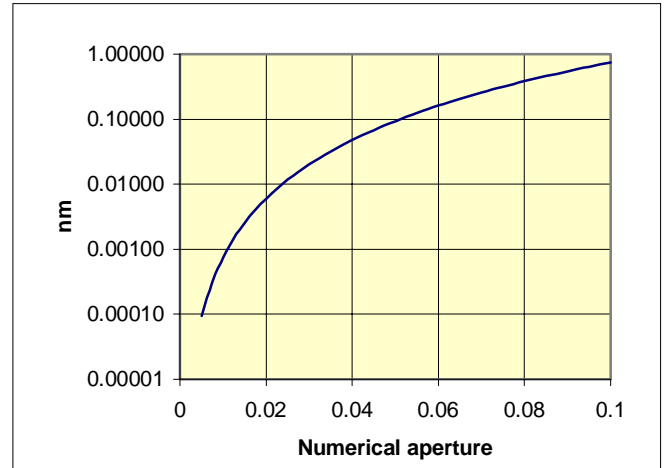
Fig. 4. Geometric coma induced error in waves as a function of NA ($s = 4.5$ μm).

measurement accuracy of $\lambda/100$ at typical EUV wavelengths (13.4 nm). Noting that the geometric coma term is parallel to the tilt component ($\rho \cos\theta$) of the path length difference [Eq. (1)], removal of the coma involves both determination of the NA of the measurement and the identification of the tilt orientation.
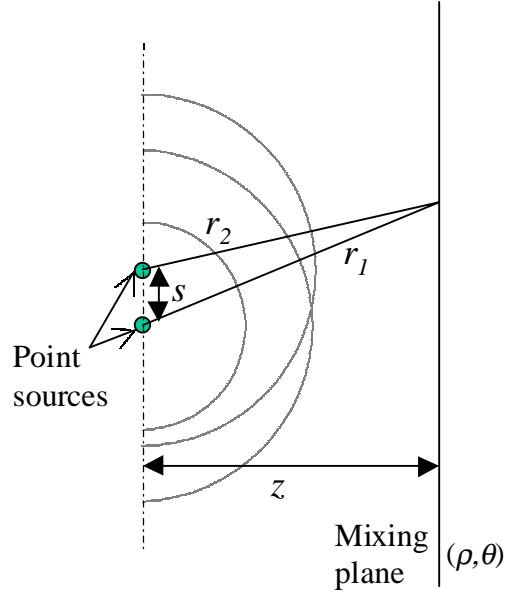
5. DETECTOR MISALIGNMENT SYSTEMATIC EFFECT

Another potential source of geometric measurement error arises from the planar detector alignment with respect to the central ray of the optical system. Proper alignment, as was assumed above, requires the detector plane to be perpendicular to the optical system central ray. The effect of misalignment as depicted in Fig. 5 can be analyzed by repeating the analysis above taking into consideration the x and y tilt of the mixing plane, γ_x and γ_y respectively, and again assuming the point separation in the image plane to lie along the x-axis.

Analysis shows the primary effect of detector tilt to be astigmatism in the measurement. Also, as might be expected, the effect of the tilt is different for tilt perpendicular to the image point separation (γ_y in our example) and tilt parallel to the point separation (γ_x). Tilt parallel to the separation has the additional effect of causing defocus. The primary path length error due to the tilt can be written as

$$\Delta R = \frac{s\rho^2}{2z^2}\left[\gamma_x(\cos 2\theta + 1) - \gamma_y \sin 2\theta\right]. \quad \textbf{(4)}$$

From Eq. (4) we find the detector-tilt-induced astigmatism error to have a magnitude of

$$e_a \approx \tfrac{1}{2}s\,NA^2\sqrt{\gamma_x{}^2 + \gamma_y{}^2} \qquad \textbf{(5)}$$

and the tilt induced defocus error to have a magnitude of

$$e_d \approx \tfrac{1}{2}s\,\gamma_x\,NA^2, \qquad\qquad \textbf{(6)}$$

where again we have used the small angle approximation to express $NA \approx r_m/z$. Considering the typical experimental values of $s = 4.5\ \mu m$ and $NA = 0.08$, we see the astigmatism error magnitude to be ~0.25 nm (0.019 waves) per degree of tilt.
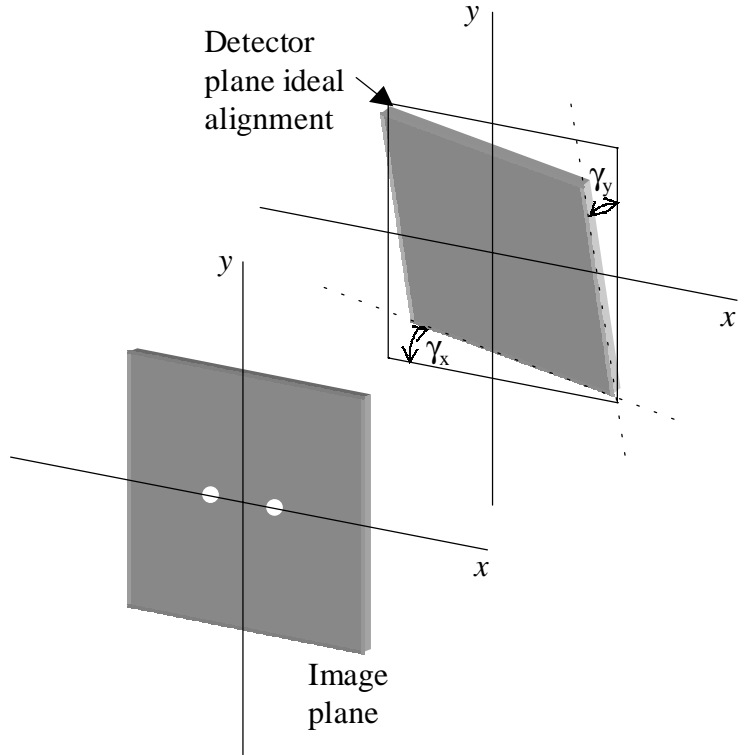

Fig. 5. Geometry for predicting the detector tilt induced systematic astigmatism error.

6. REFERENCE PINHOLE INDUCED ERRORS

The question of reference pinhole induced errors is much more subtle than the measurement geometry effects discussed above. These errors depend both on the quality of the pinholes and on the quality of the optic under test. The quality of the optic under test plays an important role because the purpose of the reference pinhole is to spatially filter the point spread function (PSF) of the optic to produce the reference beam. The greater the magnitude of the aberrations present in the optic, the more crucial this spatial filtering process becomes. From this argument, we see that it becomes easier to achieve some given accuracy as the quality of the optics being tested improves.

It is also reasonable to assume that the optic-induced errors partially decorrelate as a function of pinhole position. This allows the accuracy of the PS/PDI to be improved through an averaging process wherein the pinhole position is slightly changed (a fraction of the optic PSF) between consecutive measurements. Also, errors caused primarily by random defects in the pinhole can be reduced by taking measurements over an ensemble of equivalently sized pinholes and averaging. Here we experimentally demonstrate only the optic-induced error reduction method.

7. EXPERIMENTAL RESULTS

The accuracy of the PS/PDI has been experimentally characterized in the 10×-demagnification Schwarzschild configuration depicted in Fig. 1. For alignment purposes, the interferometer was modified to allow for *in situ* adjustment of the grating rotation and height. A variety of null-masks with various pinhole sizes were used including the 120-nm pinhole null-mask shown in Fig. 2(b). The pinhole separation in each case was 4.5 µm. The object pinhole was a 0.5-µm laser drilled pinhole. The coherent illumination was provided by a synchotron undulator beamline source (CXRO beamline 12.0.1.2 at the Advanced Light Source, LBNL)[8] operating at 13.4 nm with a bandwidth of $\lambda/\Delta\lambda \approx 200$.

Figure 6 shows an actual null test interferogram recorded on an EUV CCD using a 100-nm pinhole null-mask. The full 1"-square CCD area is shown and the image has been intensity equalized in order to reveal the quality of the fringes all the way to the edges of the CCD. The extremely straight fringes are indicative of the accuracy of the interferometer. Recovering the phase from this interferogram yields the wavefront shown in Fig. 7. As expected, the dominant term is coma in the direction of the pinhole separation. Analysis of the wavefront over a circular subaperture with an *NA* of ~0.08 (the design *NA* of the Schwarzschild system, depicted by the dotted outline in Fig. 7) shows the magnitude of the coma to be 0.029 waves zero-to-peak (0.39 nm) or 0.010 waves rms (0.13 nm).
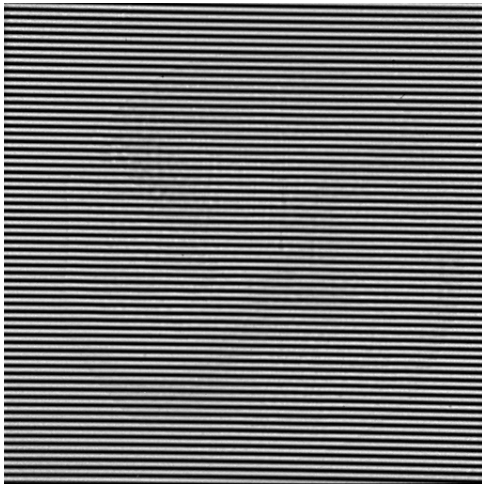

Fig. 6. Representative null test interferogram using 100 nm pinhole null-mask (full 1" square CCD image, 512×512 pixels).
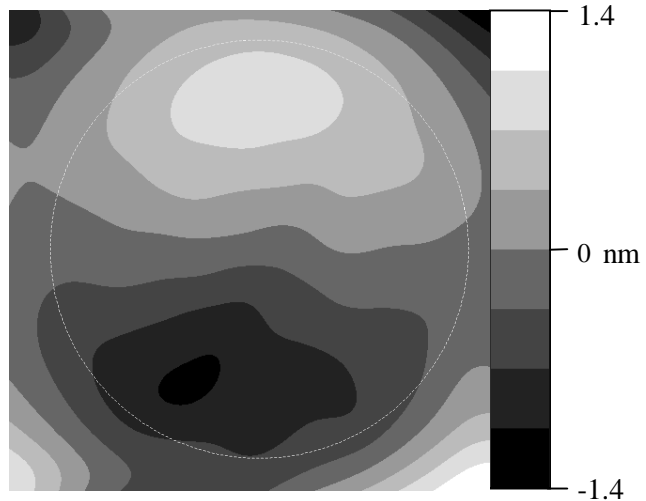

Fig. 7. Reconstructed wavefront from interferogram in Fig. 6 quantized to 8 gray levels.
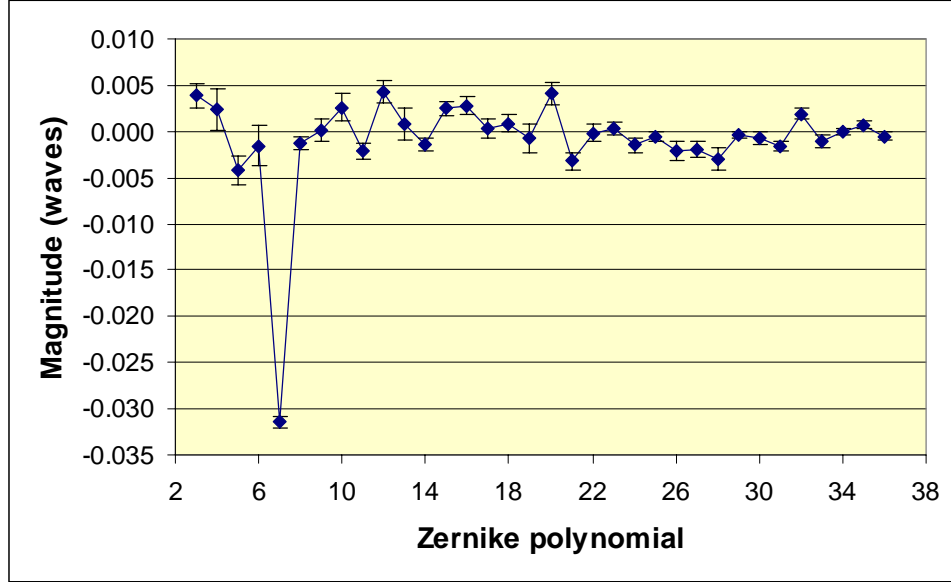
Fig. 8. Average and standard deviation of Zernike polynomial fit to 20 independent measurements.

In order to determine the accuracy of the interferometer, the measurement was repeated 20 times with small arbitrary displacements of the reference pinhole (<50 nm from the nominal position) between measurements. Figure 8 shows a plot of the average of the Zernike polynomial fits to the 20 individual wavefronts. The error bars represent the standard deviation of the 20 individual Zernike polynomial fits. As was witnessed by Fig. 7, the dominant term in the Zernike fit is coma in the direction of the pinhole separation and its average value has a magnitude of 0.031 ± 0.001 waves (0.42 ± 0.01 nm). To find the predicted geometric coma magnitude we turn to Eq. (2) for which we need the lateral measurement size, r_m, and the distance to the CCD, z. The wavefront analysis was performed over 446^2 2×2 binned pixels (48 μm per super-pixel), therefore r_m is 10.7 mm. The distance from the image plane to the CCD was experimentally determined to be 132 mm, and the pinhole separation (s) is 4.5 μm. From Eq. (2), we find the predicted geometric coma magnitude to be 0.030 waves (0.40 nm) and the measurement

NA to be 0.081. The average measured coma differs from the predicted value by only 0.001 waves (λ/1000 or 0.01 nm).

Removing the predicted geometric coma term from the wavefront in Fig. 7 we find the rms of the residual wavefront to be 0.0047 waves (λ/210 or 0.063 nm). The expected accuracy of a single measurement, however, is more accurately considered as the average residual rms from the set 20 independent measurements. Performing this average yields a single-interferogram accuracy of 0.0059 waves rms (λ/170 or 0.080 nm). This accuracy can be taken as the systematic-plus-random-error limited accuracy. However, as noted above, the measurement accuracy can be further improved through an averaging process on the wavefronts. Upon averaging, random wavefront errors will tend to cancel leaving only the systematic errors. The plot in Fig. 9 shows the residual wavefront rms (after removal of
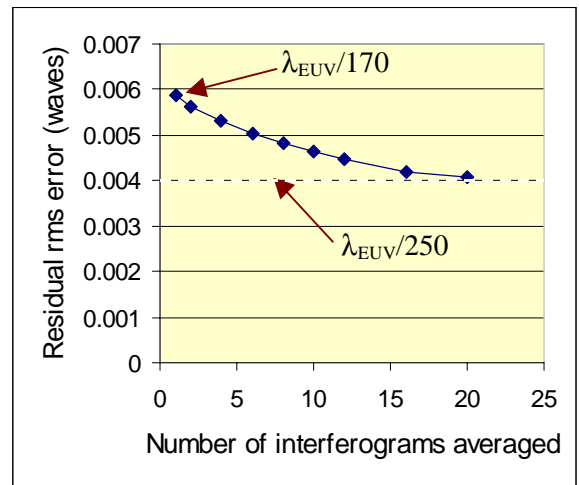

Fig. 9. Residual rms error after removal of predicted geometric coma term as a function of wavefront averaging.

the predicted geometric coma) as a function of the number of measurements averaged. As expected, the accuracy improves with averaging and asymptotically approaches 0.004 waves rms ($\lambda/250$ or 0.05 nm). We take this to be the systematic error limited accuracy of the interferometer. Figure 10 shows the average wavefront both prior to removal of the geometric coma [Fig. 10(a)] and after removal of the geometric coma [Figs. 10(b),(c)]. Figure 10(b) is displayed on the same color scale as Fig. 10(a) whereas Fig. 10(c) has been rescaled to reveal finer structure in the wavefront.

The other potential systematic geometric effect identified above was detector tilt, which potentially contributes astigmatism to the measurement. Examining the average Zernike polynomial fit in Fig. 8 we observe no significant tilt-based effects. If there existed a significant detector tilt in the direction of the point separation, we would expect the mean amplitudes of Zernike polynomials 3 and 5 to be similar [Eq. (4)]. Figure 8 shows these two terms to have mean amplitudes that are about 1.5 standard deviations (σ) away from zero, with opposite sign from each other. Similarly for Zernike polynomial 4, the term linked to tilt perpendicular to the point separation, we see that the mean is only about $1/2\ \sigma$ away from zero. If present, astigmatism due to detector tilt is limited to a magnitude below ~0.005 waves (0.07 nm). This suggests the detector alignment is correct to better than 4 mrad, an accuracy that is readily achieved with standard machining techniques. We note that a dual orientation measurement configuration where the null test is repeated with a rotation of the pinholes could help separate low-level measurement-geometry based systematic effects from systematic errors due to incomplete spatial filtering of the optic aberrations.

The results presented above were obtained using a 100-nm pinhole null-mask. It is also important to consider the accuracy as a function of pinhole size. To this end the experiment was repeated with two other null-masks, containing pairs of 120-nm pinholes and 140-nm pinholes, respectively. Table 1 shows the single measurement accuracy (calculated the same way as above) at a measurement *NA* of 0.081, as a function of pinhole size. As expected the accuracy degrades as the pinhole size increases.
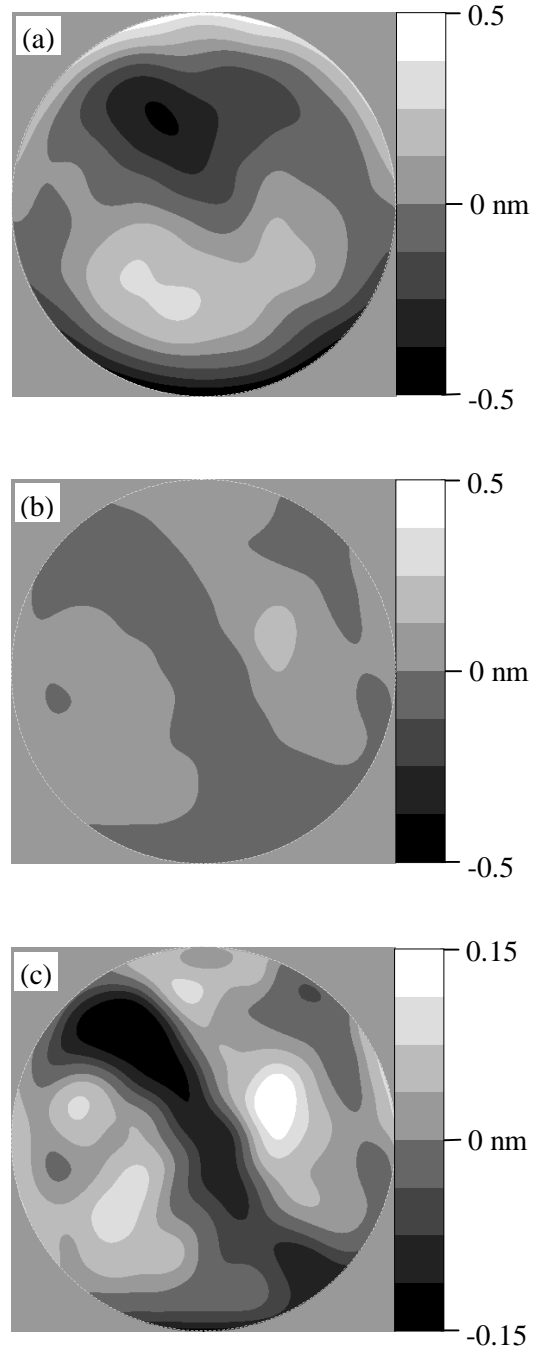

Fig. 10. Average wavefront displayed as 8 level grayscale: (a) prior to predicted geometric coma removal and (b) after predicted geometric coma removal. (c) is a rescaled version of (b) to accentuate the wavefront structure.

Earlier EUV pinhole diffraction simulations[9] with perfect input illumination predict a reference wavefront error one order of magnitude smaller than the measurements presented here. We infer that the measured aberrations are primarily due to aberrations from the optic not being sufficiently filtered by the pinholes. This suggests the accuracy will further improve as the quality of the test optic improves. EUV PS/PDI characterization of the Schwarzschild objective used in these tests showed the objective to have an rms wavefront error of ~0.2 waves over an image side *NA* of 0.08.

Another good measure of whether or not the pinholes are small enough to properly filter the optic aberrations is the coma term in the direction of the point separation. Table 1 shows this coma term as a function of pinhole size along with the error relative to the predicted value. Based on Table 1 we see the 120 nm pinhole to be adequate for measurement *NA*s of up to 0.08 and the 100 nm pinhole to far exceed the preliminary accuracy goals of EUV lithographic optic testing accuracy goal of $\lambda/100$ for the 0.08 *NA* 10×-demagnification Schwarzschild case.

Pinhole Size (nm)	Accuracy (waves)	Measured coma magnitude (waves)	Coma error relative to predicted coma magnitude (waves)
140	0.014 (0.18 nm or $\lambda/74$)	0.021 (0.28 nm)	0.009 (0.1 nm or $\lambda/100$)
120	0.011 (0.14 nm or $\lambda/94$)	0.025 (0.34 nm)	0.005 (0.07 nm or $\lambda/200$)
100	0.0059 (0.079 or $\lambda/170$)	0.031 (0.42 nm)	0.001 (0.01 nm or $\lambda/1000$)

Table 1. Accuracy and coma in the direction of point separation as a function of null-mask pinhole size.

8. CONCLUSION

The PS/PDI has previously been shown to be a highly precise measurement system.[1] Here we have demonstrated that it is also of accuracy surpassing the preliminary goals of EUV lithographic optic testing requirements. Our ability to predict, measure, and hence remove the largest systematic effect (geometric coma due to the lateral separation of the test and reference beams) has been demonstrated. Having calibrated the interferometer on the presence of this coma term, we have demonstrated an accuracy of 0.004 waves ($\lambda/250$ or 0.05 nm) in the 10×-demagnification Schwarzschild testing configuration over a measurement *NA* greater than 0.08 (the design *NA* of the Schwarzschild system).

9. ACKNOWLEDGMENTS

10. REFERENCES

1. D. M. Williamson, "The elusive diffraction limit," *OSA Proceeding on Extreme Ultraviolet Lithography*, Optical Society of America, Washington, D.C., **23**, 68-76 (1994).
2. J. E. Bjorkholm, et al.,"Phase-measuring interferometry using extreme ultraviolet radiation," J. Vacuum Science & Tech. B, **13** (6), 2919-2922 (1995).

3. A. K. Ray-Chaudhuri, et al., "Alignment of a multilayer-coated imaging system using extreme ultraviolet Foucault and Ronchi interferometric testing," J. Vacuum Science & Tech. B, **13** (6), 3089-3093 (1995).
4. E. Tejnil, *et al*., "At-wavelength interferometry for EUV lithography," J. Vacuum Science & Tech. B, **15**, 2455-2461 (1997).
5. K. A. Goldberg, *et al*., "Characterization of an EUV Schwarzschild objective using phase-shifting point diffraction interferometry," *Proceedings SPIE*, **3048**, 264-270 (1997).
6. E. Tejnil, *et al*., "Phase-shifting point diffraction interferometry for at-wavelength testing of lithographic optics," *OSA Trends in Optics and Photonics: Extreme Ultraviolet Lithography*, Optical Society of America, Washington, D.C., **4**, 118-123 (1996).
7. K. A. Goldberg, "Extreme Ultraviolet Interferometry," doctoral dissertation, Department of Physics, University of California, Berkeley (1997).
8. D. Attwood, *et al.*, "Undulator radiation for at-wavelength interferometry of optics for extreme-ultraviolet lithography," Appl. Opt. **32**, 7022-7031 (1993).
9. K. A. Goldberg, et al., "A 3-D numerical study of pinhole diffraction to predict the accuracy of EUV point diffraction interferometry," *OSA Trends in Optics and Photonics*, Optical Society of America, Washington, D.C., **4**, 133-137 (1996).